Organic & Biomolecular Chemistry

Dynamic Article Links

Cite this: *Org. Biomol. Chem.*, 2011, **9**, 6963

www.rsc.org/obc

PAPER

Cyclopenta[*c*]selenophene based cooligomers and their polymers: comparative study with thiophene analogues†

Soumyajit Das, Anjan Bedi, G. Rama Krishna, C. Malla Reddy and Sanjio S. Zade*

Received 31st May 2011, Accepted 20th July 2011
DOI: 10.1039/c1ob05866e

Selenophene and thiophene capped cyclopenta[*c*]selenophenes were synthesized and characterized. Crystal structure determination of some representative compounds revealed that the substitution at 3,4-position in the form of cyclopentane ring of selenophene or thiophene does not make any significant twist in the trimer backbone, making the cooligomer nearly planar. All the cooligomers were electrochemically polymerized and compared with thiophene capped cyclopenta[*c*]thiophene polymer. DFT calculations predict that the cyclopentane substitution on the third repeating unit (and in general) of one dimensional polymer neither disturb the planarity nor causes any significant twist on the polymeric backbone unlike the 3,4-dialkyl substitution. The electrochemically prepared selenophene based polymers showed low band gap compared to that of thiophene analogues. Cyclopentane substitution on selenophene as well as thiophene makes the resulting polymer oxidatively more stable when compared to more familiar poly-ethylenedioxythiophene (PEDOT) or poly-ethylenedioxyselenophene (PEDOS) systems. Alternate polymers of cyclopenta[*c*]selenophenes (CPS)/cyclopenta[*c*]thiophene (CPT) and thiophene/selenophene possess the energy of HOMO and LUMO significantly lower than that of homopolymers of CPS and CPT, however, possess higher band gap than PCPS.

Introduction

The first discovery of metallic conductivities in "doped" polyacetylene in 1977,[1] opened the research on conducting polymers[2] which have acquired importance both academically and industrially. Since then many aromatic systems, like thiophene, furan, aniline, azulene, indole, *para*-phenylene, as well as many substituted, multi-ring and polynuclear aromatic hydrocarbon systems, have been found to undergo electropolymerization to produce conducting polymers. Among the many compounds that have been investigated polythiophene (PT) derivatives have received increasing attention because of their good chemical stability and the advantages of their electrochemical synthesis. Thus, PT derivatives were used as materials for smart windows,[3] mirrors,[4] electrochromic devices,[5] light emitting diodes,[6] and photovoltaic cells.[7] Lack of proper synthetic methods for substituted selenophenes and a well-defined electrochemical response by polyselenophene (PSe) (which may be due to their instability during oxidative polymerization) have somehow hampered their study and applications.[8] Despite myriads of papers were published on polythiophenes, polyselenophene have recently acquired attention relying on its conductivity as a novel class of π-conjugated material exhibiting promising optoelectronic properties.[9] Structural modification is the keystone in order to tune band gap, and thus the optical and electronic properties which is possible by replacing S atom with the lower electronegative and more polarizable Se atom.[10,11] PSe derivatives exhibited excellent characteristics for electrochromic materials and are better in some aspects than the related PT derivatives.[12] Theory[13] predicted some possible advantages of PSe over PT like better inter-chain charge transfer due to intermolecular Se···Se interactions, lower oxidation and reduction potentials, accommodation of more charge upon doping due to the bigger size of selenium, lower band gaps and, consequently, lower oxidation potential (which offers high quality polymer films during electropolymerization because of minimal harmful effects of high potential; such as over oxidation may lead to degradation of the polymer). In addition, selenophene is more prone to electrophilic substitution[14] than that of thiophene. These showed that mere change of heteroatoms[11,15] in similar systems can differ greatly in their electronic properties, chemical stability and ease of polymerization. Similar to 3,4-ethylenedioxy substitution and in contrast to 3,4-dialkyl substitution in the form of two separate alkyl chains or six-membered or higher rings, 3,4-cyclopentane substitution[11] does not disturb the planarity of the resulting conjugated polymer.

Electrochemical characterization of new low band gap polyselenophenes have recently gained high attention, especially Bendikov and co workers have made great headway recently with

Department of Chemical Sciences, Indian Institute of Science Education and Research, Kolkata, PO: BCKV campus main office, Mohanpur, 741252, Nadia, West Bengal, India. E-mail: sanjiozade@iiserkol.ac.in

† Electronic supplementary information (ESI) available. CCDC reference numbers 827541 and 827542. For ESI and crystallographic data in CIF or other electronic format see DOI: 10.1039/c1ob05866e

selenophene based polymers and as of now, until our first report on dimethoxymethyl derivative of poly-cyclopenta[*c*]selenophene (CPS),[11] there are no reports on synthesis as well as the electropolymerisation of CPS based cooligomers. Herein, we extended our previous synthetic approach by showing an elegant manner to obtain an important class of chalcogen-containing heterocycles. The chalcogenophene synthesis is an important goal in organic chemistry in view of use of these compounds in the fields of biochemistry, physical organic chemistry, materials chemistry and organic synthesis. The synthesis of selenophene and thiophene derivatives, described here, is straightforward and moreover all the reactions proceeded cleanly under mild conditions. In addition to the electrochemical polymerization, structure–property correlation of PSe is discussed and compared with analogous PT.

Experimental Section

Diethyl malonate and *n*-BuLi (1.6 M in hexane) was purchased from Merck (India) and Neo-Synth respectively and used as received. Cp_2ZrCl_2, Me_3SiCl, tetrabutylammonium perchlorate, (TBAPC) and *N*-bromosuccinimide were obtained from Aldrich, and they were used as received. S_2Cl_2 was bought from Merck (Germany) and $SeCl_2$ was prepared using a reported[16] procedure. Tetrahydrofuran was distilled from sodium/benzophenone under an atmosphere of dry nitrogen. Acetonitrile (ACN, Merck, India) was distilled from P_2O_5 (Spectrochem, India) under dry nitrogen atmosphere. The other chemical reagents were common commercial products and used as received without any purification. All reactions were carried out under nitrogen. NMR spectra were recorded on either Jeol JNM-ECS400 MHz spectrometer or 500 MHz spectrometer (Brüker) as a solution in $CDCl_3$ with tetramethylsilane (TMS) as the internal standard, chemical shifts (δ) are reported in parts per million. Columns were prepared with silica gel (60–120 mesh or 230–400 mesh, Merck, India). Ferrocene powder (Sigma–Aldrich) was used to establish an electrochemical reference. Non-aqueous Ag/AgCl wire was prepared by dipping silver wire in a solution of $FeCl_3$ and HCl. Electrochemical studies were carried out with a Princeton Applied Research 263A potentiostat using platinum (Pt) disk electrode as the working electrode, a platinum wire as counter electrode, and an AgCl coated Ag wire, which was directly dipped in the electrolyte solution, as the reference electrode. Pt disk electrodes were polished with alumina, water, acetone and was dried with nitrogen gas before use to remove any incipient oxygen. The electrolyte used was 0.1 M TBAPC in ACN. Electropolymerization was done on indium tin oxide (ITO) coated glass as a working electrode. The polymer films were deposited on ITO coated glass electrode with dimensions of 5 cm × 0.7 cm at monomer's first oxidation potential (V) *vs.* Ag/AgCl and a passing charge of 100 mC or 250 mC in 0.1 M TBAPC/ACN:water (4 : 1) or 0.1 M TBAPC/ACN. Before examining the optical properties of polymer films, the films were rinsed with acetonitrile. UV-vis-NIR spectra were recorded on a HITACHI U-4100 UV-vis-NIR spectrophotometer. In spectrochemical measurements, the working electrode was an ITO-coated glass slide, the counter electrode was a platinum wire, and non-aqueous Ag/AgCl was used as the reference electrode. $E_{1/2}$ for ferrocene was calculated to be 0.29 V in ACN *versus* Ag/AgCl under these conditions. All electrochemical potentials were reported against Ag/AgCl.

Synthesis of 2

To Cp_2ZrCl_2 (755 mg, 2.58 mmol) in 40 mL of dry THF was added *n*-BuLi (3.3 mL, 5.16 mmol, 1.6 M in hexanes) at –78 °C. After the solution was stirred for about 10 mins, 4,4-bis(methoxymethyl)-1,7-bis(trimethylsilyl)hepta-1,6-diyne **6** (0.8 g, 2.46 mmol) in 5 mL of dry THF was added dropwise. The resulting solution was allowed to warm to room temperature, and stirred for additional 2 h. The color of the solution changed from pale yellow to orange. S_2Cl_2 (238 µl) was added slowly *via* syringe at 0 °C, and the solution was stirred for overnight. The reaction mixture was worked up using 3 N HCl and extracted with diethylether. Solvent was evaporated and column chromatographed quickly using hexanes first and then 2% ethylacetate in hexanes. The product recovered[17] was further desilylated with tetrabutylammonium fluoride (TBAF) in THF at ambient condition. Reaction mixture was worked up with water, diethylether and brine and after evaporating diethylether product was purified by 5% ethylacetate/hexanes mixture. Product came as liquid (130 mg, yield = 20%) but solidified on standing in refrigerator after few hours. Melting point = 38–42 °C; λ_{max} = 240 nm, (ε = 6220 $M^{-1}cm^{-1}$); ^{1}H NMR (500 MHz, $CDCl_3$): δ 6.74 (s, 2H), 3.36 (s, 4H), 3.34 (s, 6H), 2.59 (s, 4H); ^{13}C NMR (125 MHz, $CDCl_3$): δ 146.6, 114.8, 75.9, 59.2, 55.0, 33.1; HRMS calculated for $C_{11}H_{16}O_2S$ $[M]^+$, 212.0871; found 212.0242.

Synthesis of 7

2-Iodoselenophene[18] (5.98 g, 23.3 mmol), 4,4-bis(methoxymethyl)hepta-1,6-diyne **5** (2 g, 11.09 mmol), $Pd(PPh_3)_4$ (231 mg, 0.2 mmol) and CuI (38 mg, 0.2 mmol) were stirred in 30 mL of dry THF under nitrogen. To this solution was added 20 mL of diisopropylamine. The resulting solution was stirred for 48 h at rt. The mixture was filtered through celite pad. Filtrate was diluted with 30 mL diethylether and washed with 10% NH_4OH, water, 2 N HCl, water and brine. The organic layer was separated and dried over sodium sulfate. After the volatile material was removed by rotary evaporation, the residue was subjected to column chromatography (230–400 mesh silica gel, 1% ethylacetate/hexanes). Compound was isolated as colorless sticky liquid (2.4 g, yield = 49%). λ_{max} = 269 nm, (ε = 16500 $M^{-1}cm^{-1}$); IR (KBr, cm^{-1}): 3098, 3060, 2921, 2217 (C≡C), 1444, 1238, 1180, 1110, 969, 832, 791, 687; ^{1}H NMR (500 MHz, $CDCl_3$): δ 7.90 (dd, J = 5.6 Hz, 0.8 Hz, 2H), 7.31 (d, J = 3.2 Hz, 2H), 7.17 (dd, J = 5.6 Hz, 3.7 Hz, 2H), 3.44(s, 4H), 3.38 (s, 6H), 2.62 (s, 4H); ^{13}C NMR (125 MHz, $CDCl_3$): δ 133.4, 131.8, 129.2, 128.3, 92.7, 78.1, 74.0, 59.5, 42.9, 23.6; HRMS calculated for $C_{19}H_{20}O_2Se_2$ $[M+Na]^+$, 462.9691; found 462.9678.

Synthesis of 8

2-Bromothiophene (3.98 g, 24.41 mmol), 4,4-bis(methoxymethyl)hepta-1,6-diyne **5** (2 g, 11.09 mmol), $Pd(PPh_3)_4$ (231 mg, 0.2 mmol) and CuI (38 mg, 0.2 mmol) were stirred in 30 mL of dry THF under nitrogen. To this solution was added 20 mL of diisopropylamine. The resulting solution was warmed at 55 °C for 24 h using oil bath. The mixture was filtered through celite pad. Filtrate was diluted with 50 mL diethylether and washed with 10% NH_4OH, water, 2 N HCl, water and brine. The organic layer was separated and dried over sodium sulfate. After the volatile material was removed by rotary evaporation, the residue was

subjected to column chromatography (230–400 mesh silica gel, 1% ethylacetate/hexanes). A light yellow sticky pure liquid product was isolated. (2.8 g, yield = 74%). λ_{max} = 271 nm, (ε = 20000 $M^{-1}cm^{-1}$); IR (KBr, cm^{-1}): 3105, 3075, 2922, 2224 (C≡C), 1427, 1239, 1193, 1110, 980, 847, 700; ^{1}H NMR (500 MHz, $CDCl_3$): δ 7.19 (d, J = 5.1 Hz, 2H), 7.14 (d, J = 3.5 Hz, 2H), 6.94 (dd, J = 5.0 Hz, 3.6 Hz, 2H), 3.45 (s, 4H), 3.39 (s, 6H), 2.62 (s, 4H); ^{13}C NMR (125 MHz, $CDCl_3$): δ 131.1, 126.7, 126.0, 123.9, 90.7, 75.8, 74.0, 59.5, 42.8, 23.4; HRMS calculated for $C_{19}H_{20}O_2S_2$ $[M+Na]^+$, 367.0802; found 367.0865.

Synthesis of 9

To Cp_2ZrCl_2 (469 mg, 1.6 mmol) in 30 mL of dry THF was added *n*-BuLi (2 mL, 3.2 mmol, 1.6 M in hexanes) at −78 °C. After the solution was stirred for about 10 mins, 2-(4,4-bis(methoxymethyl)-7-(selenophen-2-yl)hepta-1,6-diynyl)selenophene **7** (0.67 g, 1.52 mmol) in 5 mL of dry THF was added dropwise. The resulting solution was allowed to warm to room temperature, and stirred for additional 2 h. The color of the solution changed from pale yellow to dark brown–red. $SeCl_2$ (Se = 122 mg, 1.54 mmol, SO_2Cl_2 = 126 µl, 1.54 mmol) in 2 mL dry THF was added slowly *via* syringe at 0 °C, and the solution was stirred overnight. The reaction was quenched by pouring the resulting solution into ice-cold 3 N HCl, and the resulting mixture was filtered through celite pad and then extracted with diethylether. The organic layer was washed with water and brine, and then dried over Na_2SO_4. The volatile material was then removed and the resulting dark red liquid was subjected to column chromatography (230–400 mesh, silica gel, 3% diethylether/hexanes) to get yellow solid (200 mg, yield = 25%). Melting point = 134–138 °C; λ_{max} = 386 nm, (ε = 20300 $M^{-1}cm^{-1}$); ^{1}H NMR (500 MHz, $CDCl_3$): δ 7.95 (dd, J = 6 Hz, 1 Hz, 2H), 7.24 (dd, J = 5.5 Hz, 3.5 Hz, 2H), 7.19 (dd, J = 4 Hz, 1 Hz, 2H), 3.40(s, 4H), 3.37 (s, 6H), 2.65 (s, 4H); ^{13}C NMR (125 MHz, $CDCl_3$): δ 145.7, 143.6, 131.1, 130.3, 129.8, 126.3, 75.5, 59.3, 54.3, 35.2; HRMS calculated for $C_{19}H_{20}O_2Se_3$ $[M]^+$, 517.8967; found 517.8977.

Synthesis of 10

To Cp_2ZrCl_2 (935 mg, 3.2 mmol) in 40 mL of dry THF was added *n*-BuLi (4 mL, 6.4 mmol, 1.6 M in hexanes) at −78 °C. After the solution was stirred for about 10 mins, 2-(4,4-bis(methoxymethyl)-7-(thiophen-2-yl)hepta-1,6-diynyl)thiophene **8** (1.05 g, 3.04 mmol) in 5 mL of dry THF was added drop wise. The resulting solution was allowed to warm to room temperature, and stirred for additional 2 h. The color of the solution changed from pale yellow to dark brown–red. $SeCl_2$ (Se = 243 mg, 3.07 mmol, SO_2Cl_2 = 250 µl, 3.07 mmol) in 4 mL dry THF was added slowly *via* syringe at 0 °C, and the solution was stirred overnight. The reaction was quenched by pouring the resulting solution into ice-cold 3 N HCl, and the resulting mixture was filtered through celite pad and then extracted with diethylether. The organic layer was washed with water and brine, and then dried over Na_2SO_4. The volatile material was then removed and the resulting solid was washed with hexanes to get yellow colored solid which was purified by a filter column using 2% ethylacetate in hexanes to get pure solid (400 mg, yield = 31%). Melting point = 149–153 °C; λ_{max} = 373 nm, (ε = 27200 $M^{-1}cm^{-1}$); ^{1}H NMR (500 MHz, $CDCl_3$): δ 7.23 (d, J = 5 Hz, 2H), 7.04 (d, J = 3.3 Hz, 2H), 7.01 (dd, J = 4.9 Hz, 3.8 Hz, 2H), 3.40(s, 4H), 3.36 (s, 6H), 2.69 (s, 4H); ^{13}C NMR (125 MHz, $CDCl_3$) δ 145.3, 139.1, 128.6, 127.6, 124.5, 124.1, 76.1, 59.2, 54.3, 35.3; HRMS calculated for $C_{19}H_{20}O_2S_2Se$ $[M]^+$, 424.0070; found 424.0064.

Synthesis of 11

To Cp_2ZrCl_2 (1.04 g, 3.56 mmol) in 40 mL of dry THF was added *n*-BuLi (4.7 mL, 7.5 mmol, 1.6 M in hexanes) at −78 °C. After the solution was stirred for about 10 mins, 2-(4,4-bis(methoxymethyl)-7-(thiophen-2-yl)hepta-1,6-diynyl)thiophene **8** (1.02 g, 2.97 mmol) in 5 mL of dry THF was added dropwise. The resulting solution was allowed to warm to room temperature, and stirred for additional 2 h. The color of the solution changed from pale yellow to dark brown–red. S_2Cl_2 (0.26 mL) was added slowly *via* syringe at 0 °C, and the solution was stirred overnight. The reaction was quenched by pouring the resulting solution into ice-cold 3 N HCl, and the resulting mixture was filtered through celite pad and then extracted with diethylether. The organic layer was washed with water and brine, and then dried over Na_2SO_4. The volatile material was then removed and mixture was column chromatographed (230–400 mesh silica gel, hexanes first then using 2% ethylacetate in hexanes) to get pure compound (360 mg, yield = 32%) as yellow solid. Melting point = 120–124 °C; λ_{max} = 363 nm (ε = 27100 $M^{-1}cm^{-1}$); ^{1}H NMR (400 MHz, $CDCl_3$): δ 7.22 (d, J = 5.0 Hz, 2H), 7.10 (d, J = 3.6 Hz, 2H), 7.31(dd, J = 4.8 Hz, 3.6 Hz, 2H), 3.42 (s, 4H), 3.37 (s, 6H), 2.75 (s, 4H); ^{13}C NMR (125 MHz, $CDCl_3$): δ 143.3, 137.1, 127.6, 125.2, 124.1, 123.2, 76.1, 59.2, 55.0, 34.4; HRMS calculated for $C_{19}H_{20}O_2S_3$ $[M+H]^+$, 377.0704; found 377.0796.

Synthesis of 12

N-Bromosuccnimide (76 mg, 0.42 mmol) was added in a stirred chloroform solution of **10** (90 mg, 0.21 mmol) at 0 °C. Reaction mixture was warmed to rt and left for 12 h. Saturated sodium bicarbonate solution was added and worked up using chloroform and water. Chloroform layer was dried on sodium sulfate, and solvent was evaporated to yield yellow solid (100 mg, yield = 83%). Melting point = 126–130 °C; λ_{max} = 385 nm (ε = 12500 $M^{-1}cm^{-1}$); ^{1}H NMR (400 MHz, $CDCl_3$): δ 6.95 (d, J = 3.6 Hz, 2H), 6.76 (d, J = 4.1 Hz, 2H), 3.37 (s, 4H), 3.36 (s, 6H), 2.63 (s, 4H); ^{13}C NMR (100 MHz, $CDCl_3$) δ 145.8, 140.3, 130.4, 128.0, 124.2, 111.5, 76.0, 59.2, 54.5, 35.1; HRMS calculated for $C_{19}H_{18}Br_2O_2S_2Se$ $[M+Na]^+$, 602.8178; found 602.8135.

Theoretical methods

All calculations were performed using the Gaussian 03 programe[19] at the PBC/B3LYP/6-31G(d) level. PBC/B3LYP/6-31G(d) level is method of choice to predicts the energy gaps of thiophene substances is important for a better design of the material structure.[20]

X-Ray Crystallography

Intensity data for compound **11** and **12** were collected on a Bruker's Kappa Apex II CCD Duo diffractometer with graphite monochromatic Mo-Kα radiation (0.71073 Å) at the temperature

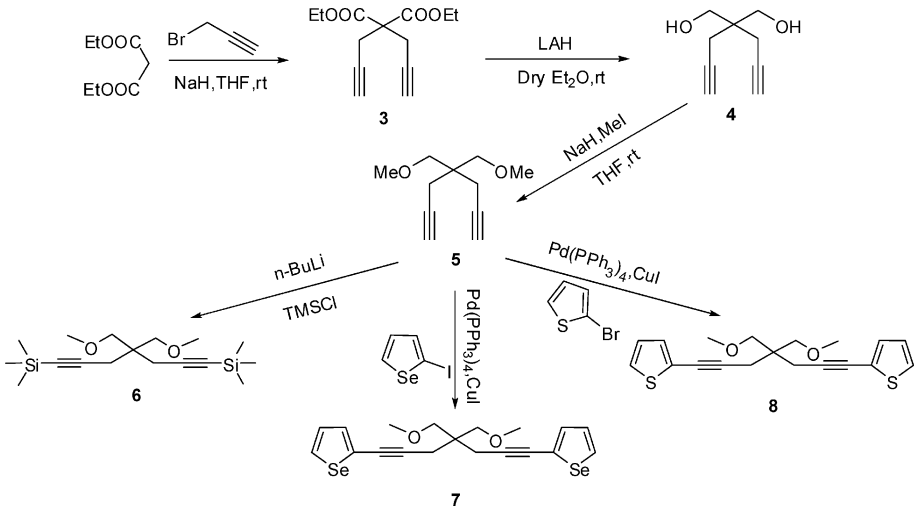

Scheme 1 Synthetic route to diyne precursors.

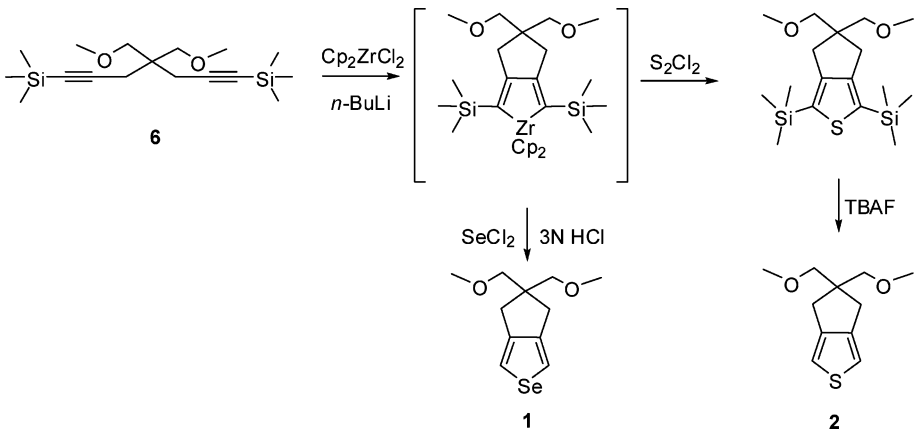

Scheme 2 Synthesis of CPS and CPT.

of 100(2) K. Scaling and multiscan absorption correction were employed using SADABS.[21] The structures were solved by direct methods and all the non-hydrogen atoms were refined anisotropically while the hydrogen atoms fixed in the predetermined positions by Shelxs-97 and Shelxl-97 packages respectively.[22] Crystal data are given in Table S6.† CCDC-827541–827542 contains the supplementary crystallographic data for compound **11** and **12**. The data can be obtained free of charge from The Cambridge Crystallographic Data Centre *via* www.ccdc.cam.ac.uk/data_request/cif.

Result and discussion

Synthesis

1,7-Bis(trimethylsilyl)-4,4-bis(methoxymethyl)-1,6-heptadiyne **6**[23] and other diyne precursors **7** and **8** were prepared in 4 steps from diethyl malonate (Scheme 1). Selenophene and thiophene derivatives of **5** were prepared by Sonogashira coupling of **5** with 2-iodoselenophene and 2-bromothiophene, respectively, as shown in the Scheme 1.

Using the same synthetic approach as reported, **6** with bis(cyclopentadienyl)-zirconium(IV) dichloride and n-butyllithium in dry tetrahydrofuran,[24,11] followed by treatment with disulfur dichloride afforded 2,5-bis(trimethylsilyl)-cyclopenta[*c*]thiophene (CPT-TMS$_2$) which was further protodesilylated to CPT **2** using TBAF in THF at rt (Scheme 2). Selenophene and thiophene capped cyclopenta[*c*]selenophene is prepared from their diaryl substituted diyne precursors **7** and **8**, respectively, using the same zirconocene coupling approach. All these cooligomers including CPT were polymerized electrochemically (Scheme 3). In addition, 2 equivalents of *N*-bromosuccnimide treatment on **10** in chloroform afforded the dibromo derivative **12** which was characterized using single crystal X-ray diffraction.

Electrochemistry and polymerisation

The CPT **2**, as expected, showed higher first oxidation potential at 1.73 V (Fig. 1a) than its Se analogue **1** (1.56 V)[11] and it is also 0.33 V higher than 3,4-ethylenedioxythiophene (EDOT). Under repeated CV cycles, **2** undergoes smooth polymerization to produce an insoluble deep blue polymer (poly(cyclopenta[*c*]thiophene)-(CH$_2$OMe)$_2$, PCPT) deposit at the surface of the platinum working electrode (Fig. 1b), following the same experimental condition as mentioned in the polymerization of CPS. Similar to CPS,[11] symmetric 3,4 substitution on thiophene inhibits any kind of unwanted cross linking, gives a planar polymer where no questions

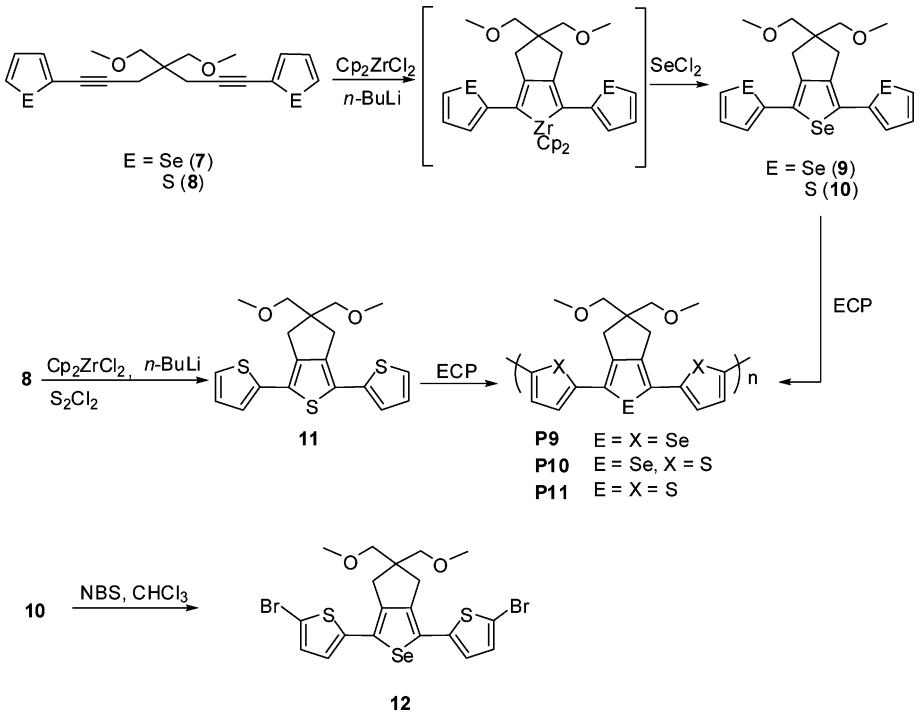

Scheme 3 Synthesis of cooligomers comprising CPS or CPT as central unit and their polymers.

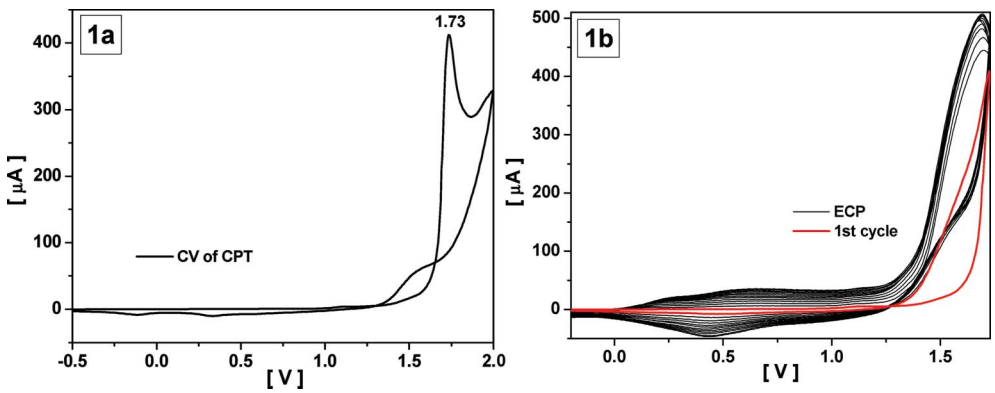

Fig. 1 (a) CV of CPT in ACN and 0.1 M $(Bu_4N)_4ClO_4$ (TBAPC) on a Pt electrode, first scan at 50 mV s^{-1} *vs.* Ag/AgCl wire. (b) Multisweep electropolymerization of CPT on a Pt electrode in ACN and 0.1 M TBAPC at 50 mV s^{-1} *vs.* Ag/AgCl wire.

on regioirregularity would arise. However, scan-rate dependence could not be studied as the PCPT is peeled off the Pt disk at higher scan rates. However, PCPS was well studied and showed well defined behavior in scan-rate dependence electroactivity.[11]

CPT was electropolymerized on an ITO coated glass electrode with dimensions of 5 cm × 0.7 cm at a constant potential of 1.8 V *vs.* Ag/AgCl and a passing charge of 250 mC in 0.1 M TBAPC/ACN. We have observed the formation of soluble red and blue oligomers during the electropolymerization. Consequently, formation of a smooth film on an ITO electrode was found to be difficult and it also supports the previously reported fact that the presence of the cyclopentane ring affects the grafting of the polymer onto the electrode.[25] However, a coating of PCPT on an ITO coated glass slide was successful after repeated attempts. The spectroelectrochemical data were recorded at various applied potentials *in situ* in the monomer-free electrolyte solution. Fig. 2a shows the absorption spectra in the UV-vis-NIR region of PCPT films at different applied potentials in acetonitrile. The optical band gap measured in spectroelectrochemical studies of PCPT (assigned as the onset of the π–π* transition) is 1.73 eV (716 nm) which is higher than PCPS (1.65 eV). DFT calculated (at PBC/B3LYP/6-31G(d)) values for the highest occupied crystal orbital (HOCO) and lowest unoccupied crystal orbital (LUCO) levels for PCPT at k = 0 are –3.94 and –1.91 eV, respectively and for corresponding selenophene analogue are –3.86 and –2.04 eV, respectively. Calculated band gap of PCPT is 2.03 eV which is again higher than PCPS (1.83 eV).[11] Calculations on dimers and polymers[11] (calculated at the same level of theory) suggest that 3,4-cyclopentane substitution does not create any steric congestion and maintains the planarity of the resulting conjugated systems, whereas 3,4-dialkyl substitutions are known to cause significant twisting of the polythiophene backbone.[25,26]

The color of PCPT ranges from deep blue in the neutral state to transmissive grey in the doped state. The formation

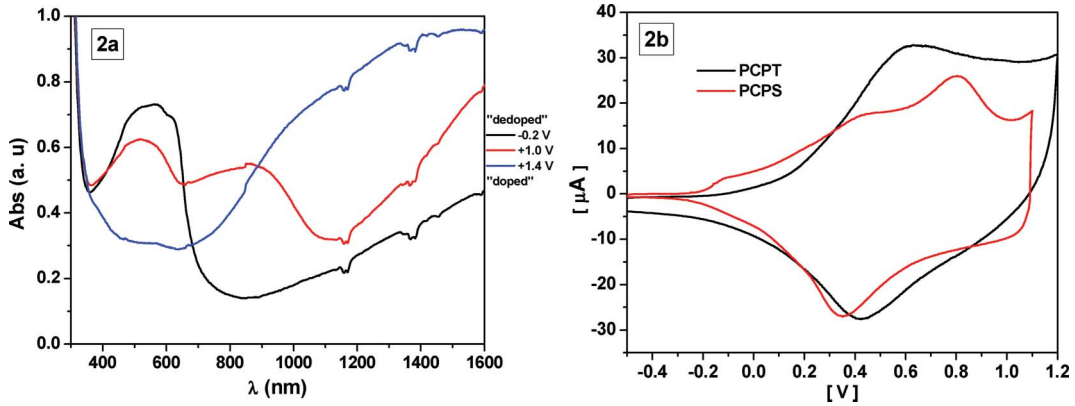

Fig. 2 (a) Spectroelectrochemistry of PCPT thin film prepared on ITO coated glass as a function of applied potential in acetonitrile. (b) CV of PCPT and PCPS studied at 50 mV s^{-1} *vs.* Ag/AgCl in ACN and 0.1 M TBAPC.

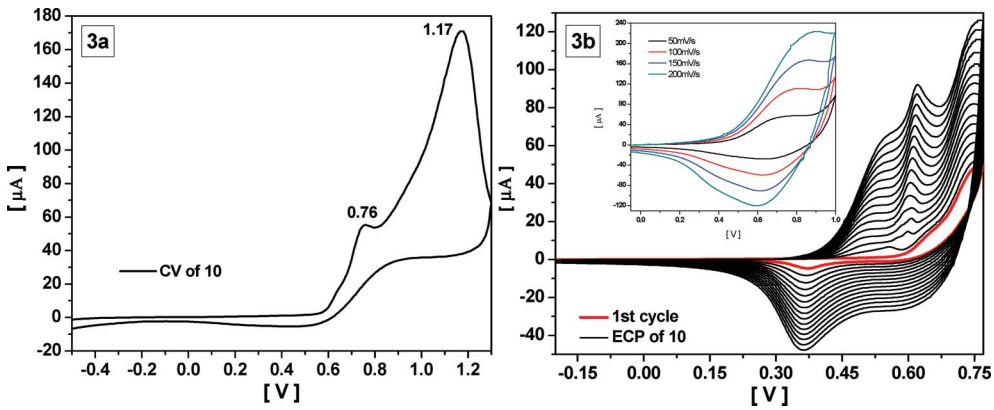

Fig. 3 (a) CV of **10** in ACN:water (4 : 1) and 0.1 M TBAPC on a Pt electrode, first scan at 50 mV s^{-1} *vs.* Ag/AgCl wire. (b) Multisweep electropolymerization of **10** on a Pt electrode in ACN : water (4 : 1) and 0.1 M TBAPC at 50 mV s^{-1} *vs.* Ag/AgCl wire. (Inset) Cyclic voltammetry of **P10** produced in monomer-free acetonitrile and 0.1 M TBAPC as a function of scan rate.

of polarons for PCPT was observed at around 900 nm while the bipolarons peak appeared at 1400 nm. The formation of polarons for PCPS was observed at around 1040 nm while the bipolarons peak was expected above 1800 nm.[11] Replacement of S by Se significantly shifted the absorption peak for polaronic and bipolaronic species. It is notable that the peak maximum of the band gap absorption of PCPS is situated at a longer wavelength than that of PCPT. The absorption maximum for PCPT is 568 nm which is lower than its selenium analogue (629 nm). Although there is significant difference in the λ_{max} values of PCPT and PCPS, the band gap values do not differ much as a result of close onset wavelength values due to broader absorption peak for PCPT than that of PCPS. The smaller band gap energy of PCPS indicates the better conjugated π-system with a longer conjugation length. The HOCO and LUCO levels of PCPS compared with the PCPT suggests that the LUMO is stabilized, while the HOMO is less affected by replacement of S with Se, hence resulting in a smaller bandgap. Although, the cyclic voltammogram showed higher onset oxidation potential for PCPT than that of PCPS, making the PCPT an effective polymer for application in bulk heterojunction solar cells (BHJ) in future.

Cyclic voltammogram of **10** in ACN:water (4 : 1)/TBAPC solvent/electrolyte couple indicated two consecutive oxidation peaks at 0.76 and 1.17 V (Fig. 3a). Upon consecutive cycle, formation a new oxidation peak appeared at 0.61 V due to the oxidation of the polymer (Fig. 3b). As the number of cycle increases, an increase in the current intensity was observed. This can be attributed to increase in the active area of the working electrode owing to electroactive polymer coating on the metal electrode. Due to the partial dissolution of neutral linear low molecular weight oligomers, a greenish-blue cloud was formed around the electrode. Under these conditions, **10** yielded an orange–red polymer which was consequently doped at the same potential to generate polarons balanced with ClO_4^- counterions and further dedoping of this polymer at 0.36 V peak involved the neutralization of polarons with the release of ClO_4^- and the resulting short linear species were dissolved. For studying the electrochemistry of the polymer, a monomer free system was used. Fig. 3b inset shows the scan rate dependence of the current response during redox cycling of **P10** between –0.2 and +0.76 V. It can be seen that both the anodic and cathodic peak currents scale linearly with scan rate which is as expected for an electrode-supported electroactive film. DFT calculations showed the resulting polymers to be almost planar. In addition, the crystal structure data shows the experimental dihedral angle of **12** (δ) is ~7–19°, indicating the thiophene substitution at the 2,5 position of CPS does not disturb the planarity of the trimer significantly.

For the spectroelectrochemical study of the **P10**, the film was deposited on an ITO coated glass electrode at a constant potential of 0.76 V *vs.* Ag/AgCl and a passing charge of 100 mC in 0.1 M TBAPC/ACN : water (4 : 1). **P10** coated ITO was then investigated by UV-vis-NIR spectroscopy in monomer free 0.1 M TBAPC/ACN system by switching the potential between –0.3 and +1.0 V. At the neutral state λ_{max} due to the π–π* transition of the polymer was 476 nm and band gap (assigned as the onset of the π–π* transition) was calculated as 1.88 eV (658 nm). Upon applied voltage, reduction in the intensity of the π–π* transitions and formation of charge carrier bands were observed at 700 nm and 1300 nm. However, at higher potential (+0.9 V) one additional band was originated at 950 nm (Fig. 4).

Cyclic voltammetry (CV) of **9** and **11** (Fig. 5a and Fig. 5b) were carried out in acetonitrile/water (4/1, v/v) solvent mixture using TBAPC (0.1 M) as the supporting electrolyte. Cyclic voltammogram of electrolytic solution containing **11**, a terthiophene unit, exhibits one irreversible oxidation peak at 0.98 V in the first anodic scan while the oxidation potential for monomer **9**, at the same condition, is shifted to 0.70 V due to the presence of three selenophene moieties and it also supports the fact that selenophene is known to lower the oxidation potential when compared to its thiophene analogue. The oxidation potential of monomer **10** (Fig. 3a) is even lower (due to the presence of a selenophene ring) than the terthiophene **11** when measured under the similar conditions.

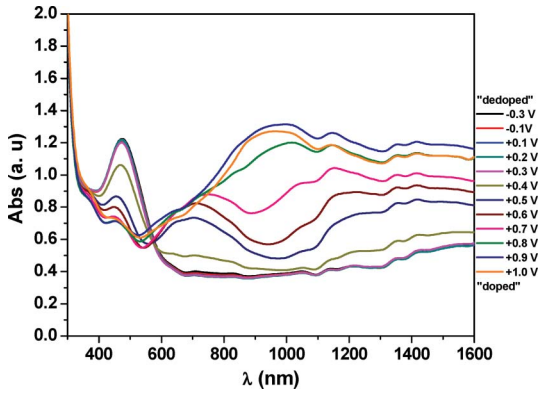

Fig. 4 Optoelectrochemical spectra of **P10** at applied potentials between –0.3 and +1.0 V in the presence of 0.1 M TBAPC in ACN.

The formation of **P9** and **P11** can be easily seen with the increasing intensity of the reversible redox couple, indicating doping and dedoping of the polymer film (Fig. 5c and Fig. 5d). Also, electrochemical behavior of the orange–red polymer film obtained from **9** and **11** after 20 repetitive cycles was investigated in the monomer-free electrolytic solution. A linear relationship

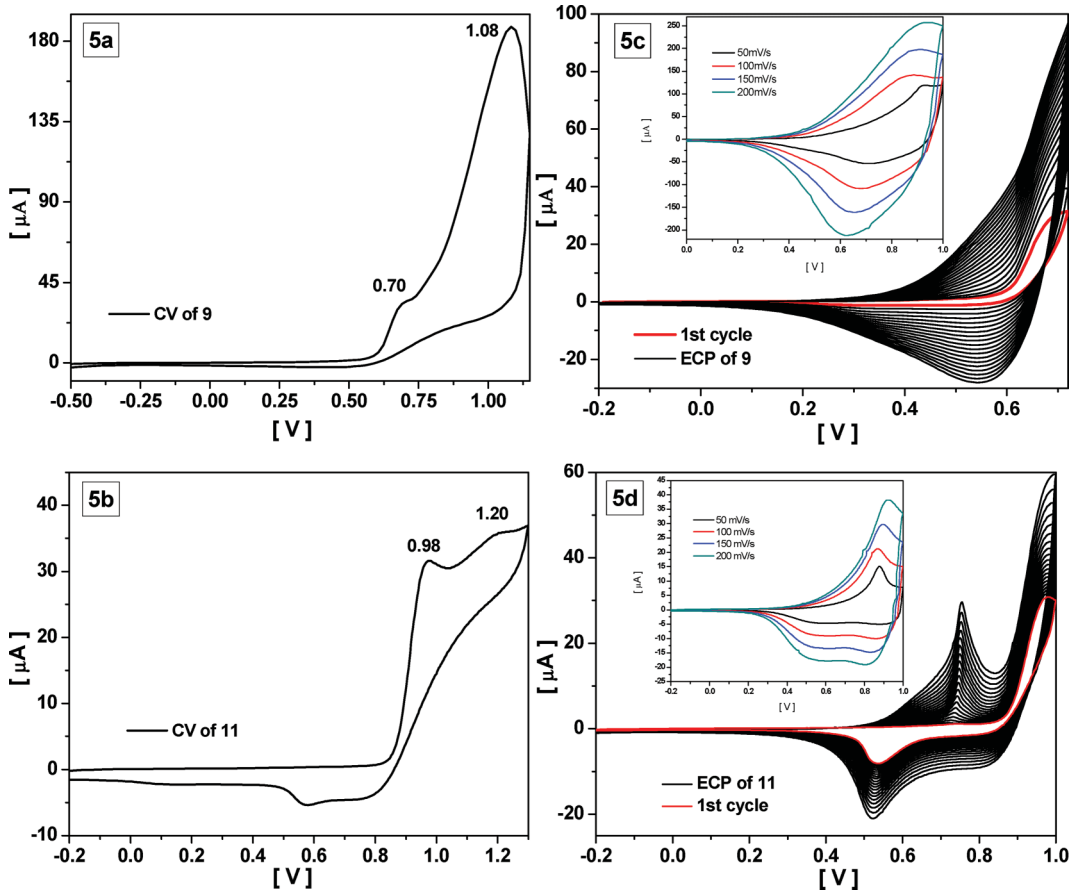

Fig. 5 (a) and (b) CV of **9** and **11**, respectively, in ACN : water (4 : 1) and 0.1 M TBAPC on a Pt electrode, first scan at 50 mV s^{-1} *vs.* Ag/AgCl wire, (c) and (d) Multisweep electropolymerization of **9** and **11** on a Pt electrode in ACN : water (4 : 1) and 0.1 M TBAPC at 50 mV s^{-1} *vs.* Ag/AgCl wire, respectively. (Inset) Cyclic voltammetry of **P9** and **P11** produced in monomer-free acetonitrile and 0.1 M TBAPC as a function of scan rate.

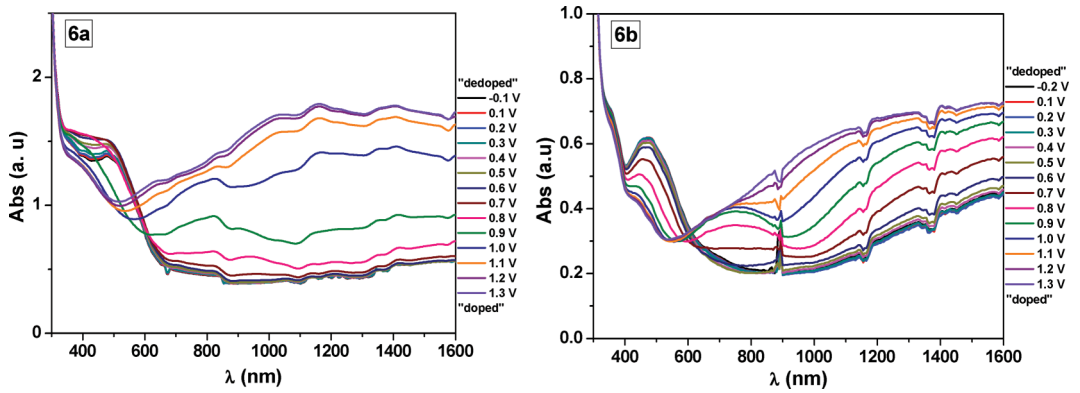

Fig. 6 (a) Spectroelectrochemistry of **P9** thin film prepared on ITO coated glass as a function of applied potential between –0.1 and +1.3 V in acetonitrile. (b) Spectroelectrochemistry of **P11** thin film prepared on ITO coated glass as a function of applied potential between –0.2 and +1.3 V in acetonitrile.

between the peak current and scan rate demonstrates that the films were well adhered and the electrochemical processes are reversible and non-diffusion-controlled.

For spectroelectrochemical measurements, polymer films were electrochemically deposited on ITO-coated glass plates from 1×10^{-2} M monomer solutions of **9** and **11** in 0.1 M TBAPC/ACN/water. The optical changes were investigated by UV-vis-NIR spectroscopy in TBAPC/ACN electrolytic system by increasing the applied potential. After polymerization, the films were rinsed with acetonitrile to remove any unreacted monomer. The changes in electronic absorption spectra recorded *in situ* at various applied potentials are depicted in Fig. 6a and 6b. The electronic absorption spectrum of the neutral form of the **P9** polymer film exhibits a band at about 480 nm due to π–π* transition and from the onset on the low energy end the band gap was found to be 1.69 eV (732 nm). This value is lower than the band gap of **P11** that appears at 1.98 eV (626 nm) and even lower than **P10** (1.88 eV, Fig. 4) and this difference might be attributed to the presence of selenium atom which stabilizes the LUMO. Beyond 0.6 V upon doping, two new bands near 820 nm for **P9** and 750 nm for **P11** as well as a band near 1200 nm start to intensify indicating the formation of polarons, and bipolarons, respectively (Fig. 6a and Fig. 6b).

The important difference of replacing the alkoxy groups (as EDOT and EDOS) for alkyl-groups is the increased oxidative stability of the polymer (high E_{ox}). The higher onset oxidation potential may lead to much lower HOMO level of the polymer which in turn may increase the open circuit voltage (V_{oc}) of solar cell. Experimentally, we found that HOMO of PCPT is more stabilized than PCPS although low band gap of PCPS indicates more conjugated system than PCPT. However, the HOMO of both PCPT and PCPS are more stabilized than PEDOT or PEDOS (Table 1). Finally, all the copolymers are regiosymmetric by nature. The experimental and theoretical HOMO, LUMO and band gap are shown in the Table 1. The calculated HOMO and LUMO energies are shown in Fig. 7. HOMO and LUMO levels in polymer **P9–P11** (alternate CPT/CPS and bithiophene/biselenophene copolymers) are significantly stabilized (by ~ 0.4–0.6 eV) compared to that of PCPS and PCPT (homopolymers). The low lying HOMO (high ionization potential) of these copolymers has implication in photovoltaic application by considering (i) stability of the resulting polymers and (ii) matching of the acceptor energy

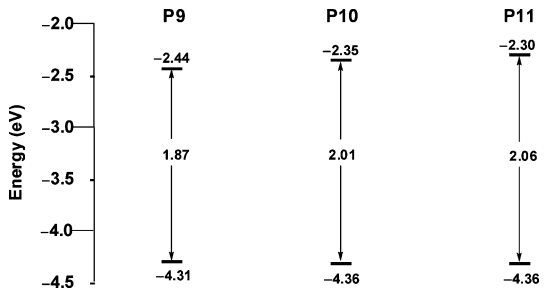

Fig. 7 Comparison of the calculated energy levels of **P9–P11** at B3LYP/6-31G(d).

levels to draw higher V_{oc} in the photovoltaic devices. Thus, this strategy can be extended to prepare the polymers in which the frontier orbital energy levels can be tuned with the energy levels of the acceptor such as fullerene to improve the performance of the photovoltaic devices. Pictorial representation (Fig. 7) indicates that the LUMO level changes significantly on changing sulfur by selenium whereas the HOMO level stays nearly at constant value. Alternate copolymers showed relatively higher band gap than that of homopolymers of CPT and CPS.

Crystal structures

The compound **11** crystallizes in the monoclinic $P2_1/c$ space group with two molecules (conformers) in the asymmetric unit in that the oligomers are nearly planar (Fig. 8). Intriguingly, one of the conformer (I) has two outer thiophene rings in *anti* relationship with the central CPT, whereas in another conformer (II) the two outer thiophene rings are in *syn* and *anti* fashion to the central CPT, respectively. The crystal structure refinement of **11** was not fully satisfactory (R factor = 15.15%) as there was some positional disorder in the outer *syn* thiophene ring of conformer II in that the thiophene ring flips 180° to lead to the partial occupancies of S1 and C3 atoms over the two positions. Our attempt to model the disorder was not successful as the subsequent refinements always resulted in unstable structures, hence the disorder modeling was not included in the final structure (Fig. 9). But, the refinements indicated that the S atom predominantly occupies the *syn* position with roughly about > 70% probability, and hence it is reasonable to treat the thiopehene ring as *syn*.[27,28] Dihedral angles between

Table 1 Calculated HOCO (Highest Occupied Crystal Orbital), LUCO (Lowest Unoccupied Crystal Orbital), energies (at at $k = 0$ using B3LYP/6-31G(d)), optical band gaps and experimental HOMO (Highest Occupied Molecular Orbital) for **P9–P11** and PCPT and PCPS

Polymers	λ_{max} (nm)	HOCO[a] (eV)	LUCO[a] (eV)	Band gap (eV)		HOMO[c] (eV)
				Calcd.[a]	Exp.[b]	
P9	480	–4.31	–2.44	1.87	1.69	–5.02
P10	476	–4.36	–2.35	2.01	1.88	–4.96
P11	478	–4.36	–2.30	2.06	1.98	–5.09
PCPT	568	–3.94	–1.91	2.03	1.73	–4.64
PCPS[11]	629	–3.86	–2.04	1.83	1.65	–4.43

[a] Calculated band gap, HOCO and LUCO. [b] Experimental optical band gap obtained from spectroelectrochemical data. [c] Experimental HOMO = – e($E_{ox,\ onset} - E_{1/2}$ (ferrocene) + 4.8) (eV).

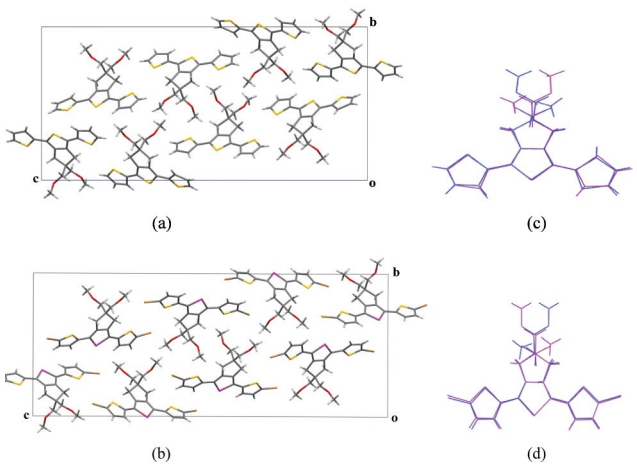

Fig. 8 Crystal packing in compounds (a) **11** and (b) **12** to show the isostructural relationship. Notice the elongation of unit cell *c*-axis in **12** due to the slight increase in molecular length along the C–Br bond projection. Overlay diagram to show the conformational differences between the two crystallographically independent conformers in compounds (c) **11** and (d) **12** (blue colour: conformer-I; purple colour: conformer-II). Notice the *syn-anti* and *ani-anti* relationship in conformer-I (blue) and II (red) in **11**, respectively, and both *anti-anti* in **12**.

the rings in conformer I are 171.6(5)° (C22-C23-C24-C25) and –174.4(5)° (C33-C34-C35-C36). In the conformer II the dihedral angles are 15.6(8)° (C3-C4-C5-C6) and 174.2(6)° (C14-C15-C16-C17) between *syn* and *anti* rings, respectively. These dihedral angles show that the outer thiophene rings are largely co-planar with the central CPT ring in both the conformers. Generally, oligothiophenes prefer the lowest energy *anti* arrangement within the rings. However in the case of conformer II, *syn* arrangement of one of the outer thiophene rings may be the result of a low flipping activation potential energy. The torsional potential of one of the capped thiophene ring in **11** was calculated by scanning a torsional angle from 0 to 180° by a step of 30° to be 3.2 kcal mol^{-1} (at B3LYP/6-31G(d)) (See SI). Additionally, transition state (TS) structure, which connect *syn* and anti conformations, calculation also afforded the similar value for the torsional potential.

In the crystal structure of **11**, the molecules along [100] are packed with $\pi\cdots\pi$ stacking interaction while there are only van der Waals forces along the other two crystallographic directions. The presence of reliable $\pi\cdots\pi$ stacking interactions in the structure makes it a dependable candidate to use as a material of semiconducting devices where planarity and well-stacked crystallinity is highly concerned.

Despite having considerable difference in the molecular structure, the compound **12** adopts the isostructural crystal packing with respect to compound **11**. The compound **12** crystallizes in the monoclinic $P2_1/n$ space group with two symmetry independent molecules in the asymmetric unit ($Z' = 2$). The two oligomers adopt the similar planar conformation, however, unlike in **11**, both the

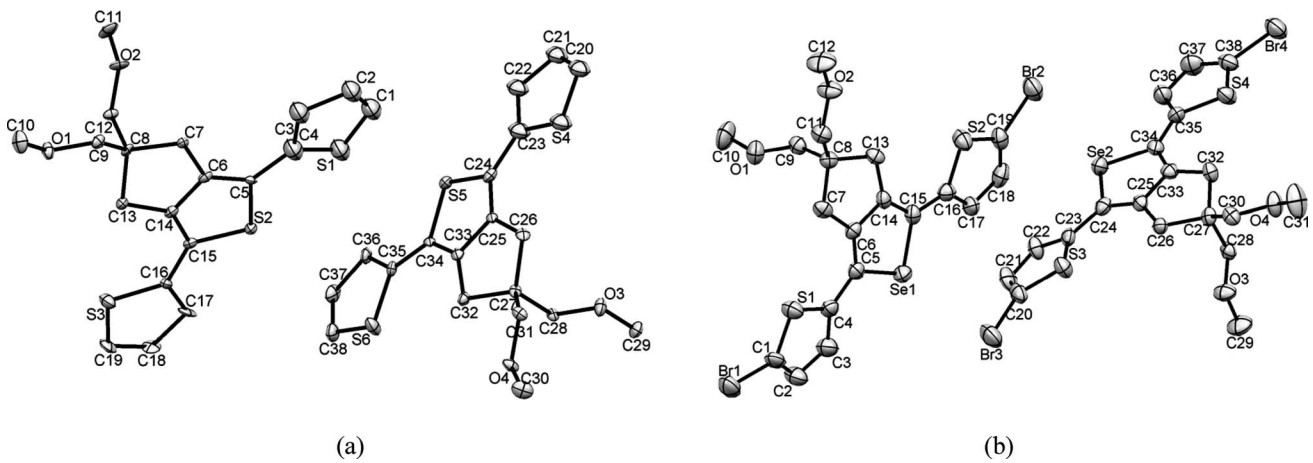

Fig. 9 ORTEP diagrams of (a) compound **11** and (b) **12**. Thermal ellipsoids are drawn at 50% probability. Hydrogen atoms on carbons are omitted for clarity.

thiophene units stay *trans* to the central CPS moiety (no disorder was found in this case) (Fig. 8). Dihedral angles between the rings are in the range of 161–173°. The short perpendicular distance of 2.94 Å between two mean planes of outer thiophene rings from the adjacent molecules shows efficient $\pi\cdots\pi$ stacking in **12**, which is considerably shorter than the same in **11** (3.30 Å). The C–Br$\cdots$O interactions in **12** connect the molecules along the crystallographic *c*-axis. The incorporation of selenium in the central moiety changes the bond angle from ~93° for **11** (C_5-S_2-C_{15} - 92.4(2)) to ~88° (C_5-Se_1-C_{15} - 87.7(2)) for **12**. The *anti-anti* conformation in both the symmetry independent molecules apparently has no influence on the overall crystal packing in **12** when compared to the *syn-anti* and *anti-anti* in compound **11**. Although the structure of **11** has high R value with some disorder, the structure clearly indicates to the high preference for planarity in these class of compounds.

Conclusion

The paper reports an elegant manner to obtain thiophene and selenophene capped CPS cooligomers using an efficient synthetic approach. For comparison, we had synthesized the thiophene capped CPT cooligomer as well as CPT. All the cooligomers were polymerized electrochemically. Single crystal XRD and DFT studies revealed the trimer and polymers are almost planar leading to highly conjugated systems. Selenophene containing polymers are having lower band gap than thiophene analogues, though the thiophene based polymers are having deeper HOMO levels due to higher onset oxidation potentials, which make these polymers more resistant against unintentional doping and effective to be applied in photovoltaic cells. Alternate copolymers of thiophene/selenophene (unsubstituted) with CPT/CPS (substituted) have significantly lower values for HOMO and LUMO levels compared to that of homopolymers of CPT/CPS.

Acknowledgements

Financial support from DST, India is gratefully acknowledged by SSZ and CMR. AB acknowledges CSIR for research fellowship.

References

1 C. K. Chiang, C. R. Fincher, Y. W. Park, A. J. Heeger, H. Shirakawa, E. J. Louis, S. C. Gau and A. G. MacDiarmid, *Phys. Rev. Lett.*, 1977, **39**, 1098–110.
2 (*a*) *Handbook of Organic Conductive Molecules and Polymers*; ed. H. S. Nalwa, John Wiley & Sons, New York, 1997; Vol. 2; (*b*) *Handbook of Conducting Polymers*, 3rd ed., ed. T. A. Skotheim and J. R. Reynolds, CRC Press, Boca Raton, FL, 2007; (*c*) *Handbook of Thiophene–based Materials: Applications in Organic Electronics and Photonics*, ed. I. F. Perepichka and D. F. Perepichka, John Wiley & Sons, New York, 2009, Vol. 1.
3 R. Rauh, *Electrochim. Acta*, 1999, **44**, 3165–3176.
4 R. J. Mortimer, *Chem. Soc. Rev.*, 1997, **26**, 147–156.
5 S. I. Cho, W. J. Kwon, S. Choi, P. Kim, S. Park, J. Kim, S. J. Son, R. Xiao, S. Kim and S. B. Lee, *Adv. Mater.*, 2005, **17**, 171–175.
6 (*a*) A. C. Grimsdale, K. Leok Chan, R. E. Martin, P. G. Jokisz and A. B. Holmes, *Chem. Rev.*, 2009, **109**, 897–1091; (*b*) I. F. Perepichka, D. F. Perepichka, H. Meng and F. Wudl, *Adv. Mater.*, 2005, **17**, 2281–2305.
7 (*a*) S. Günes, H Neugebauer and N. S. Sariciftci, *Chem. Rev.*, 2007, **107**, 1324–1338; (*b*) M. C. Scharber, D. Wühlbacher, M. Koppe, P. Denk, C. Waldauf, A. J. Heeger and C. J. Brabec, *Adv. Mater.*, 2006, **18**, 789–794.
8 A. Patra and M. Bendikov, *J. Mater. Chem.*, 2010, **20**, 422–433.
9 (*a*) K. Aydemir, S. Tarkuc, A. Durmus, G. E. Gunbas and L. Toppare, *Polymer*, 2008, **49**, 2029–2032; (*b*) K. Takimiya, Y. Kunugi, Y. Konda, N. Niihara and T. Otsubo, *J. Am. Chem. Soc.*, 2004, **126**, 5084–5085; (*c*) T. Okamoto, K. Kudoh, A. Wakamiya and S. Yamaguchi, *Org. Lett.*, 2005, **7**, 5301–5304; (*d*) B. Dong, Y. Xing, J. Xu, L. Zheng, J. Hou and F. Zhao, *Electrochim. Acta*, 2008, **53**, 5745–5751; (*e*) A. Dadvand, F. Cicoira, K. Yu. Chernichenko, E. S. Balenkova, R. M. Osuna, F. Rosei, V. G. Nenajdenko and D. F. Perepichka, *Chem. Commun.*, 2008, 5354–5356; (*f*) M. İ. Özkut, S. Atak, A. M. Önal and A. Cihaner, *J. Mater. Chem.*, 2011, **21**, 5268–5272.
10 (*a*) M. Heeney, W. Zhang, D. J. Crouch, M. L. Chabinyc, S. Gordeyev, R. Hamilton, S. J. Higgins, I. McCulloch, P. J. Skabara, D. Sparrowe and S. Tierney, *Chem. Commun.*, 2007, 5061–5063; (*b*) A. Patra, Y. H. Wijsboom, S. S. Zade, M. Li, Y. Sheynin, G. Leitus and M. Bendikov, *J. Am. Chem. Soc.*, 2008, **130**, 6734–6736; (*c*) E. Aqad, M. V. Lakshmikantham and M. P. Cava, *Org. Lett.*, 2001, **3**, 4283–4285.
11 S. Das and S. S. Zade, *Chem. Commun.*, 2010, **46**, 1168–1170.
12 (*a*) M. Li, Y. Sheynin, A. Patra and M. Bendikov, *Chem. Mater.*, 2009, **21**, 2482–2488; (*b*) M. Li, A. Patra, Y. Sheynin and M. Bendikov, *Adv. Mater.*, 2009, **21**, 1708–1711; (*c*) A. Patra, Y. H. Wijsboom, G. Leitus and M. Bendikov, *Chem. Mater.*, 2011, **23**, 896–906.
13 S. S. Zade, N. Zamoshchik and M. Bendikov, *Chem.–Eur. J.*, 2009, **15**, 8613–8624.
14 S. Das, P. K. Dutta, S. Panda and S. S. Zade, *J. Org. Chem.*, 2010, **75**, 4868–4871.
15 A. Saito, Y. Matano and H. Imahori, *Org. Lett.*, 2010, **12**, 2675–2677.
16 A. Maaninen, T. Chivers, M. Parvez, J. Pietikäinen and R. S. Laitinen, *Inorg. Chem.*, 1999, **38**, 4093–4097.
17 We had experienced a mixture of CPT–TMS_2 and CPT after column, so it was desilylated further to get only CPT. Instead of using 3 N HCl or usual work up, if reaction mixture was directly loaded on triethylamine treated silica gel, CPT–TMS_2 can be isolated. ^{1}H NMR (400 MHz, $CDCl_3$) δ 3.37 (s, 4H), 3.35 (s, 6H), 2.58 (s, 4H), 0.27 (s, 18H).
18 K. Takahashi and S. Tarutani, *Heterocycles*, 1996, **43**, 1927–1935.
19 *Gaussian 03*, Revision E.01. M. J. Frisch, G. W. Trucks, H. B. Schlegel, G. E. Scuseria, M. A. Robb, J. R. Cheeseman, J. A. Montgomery, Jr., T. Vreven, K. N. Kudin, J. C. Burant, J. M. Millam, S. S. Iyengar, J. Tomasi, V. Barone, B. Mennucci, M. Cossi, G. Scalmani, N. Rega, G. A. Petersson, H. Nakatsuji, M. Hada, M. Ehara, K. Toyota, R. Fukuda, J. Hasegawa, M. Ishida, T. Nakajima, Y. Honda, O. Kitao, H. Nakai, M. Klene, X. Li, J. E. Knox, H. P. Hratchian, J. B. Cross, C. Adamo, J. Jaramillo, R. Gomperts, R. E. Stratmann, O. Yazyev, A. J. Austin, R. Cammi, C. Pomelli, J. W. Ochterski, P. Y. Ayala, K. Morokuma, G. A. Voth, P. Salvador, J. J. Dannenberg, V. G. Zakrzewski, S. Dapprich, A. D. Daniels, M. C. Strain, O. Farkas, D. K. Malick, A. D. Rabuck, K. Raghavachari, J. B. Foresman, J. V. Ortiz, Q. Cui, A. G. Baboul, S. Clifford, J. Cioslowski, B. B. Stefanov, G. Liu, A. Liashenko, P. Piskorz, I. Komaromi, R. L. Martin, D. J. Fox, T. Keith, M. A. Al–Laham, C. Y. Peng, A. Nanayakkara, M. Challacombe, P. M. W. Gill, B. Johnson, W. Chen, M. W. Wong, C. Gonzalez, J. A. Pople, Gaussian, Inc., Wallingford CT, 2007.
20 (*a*) S. S. Zade and M. Bendikov, *Org. Lett.*, 2006, **8**, 5243–5246; (*b*) J. Gierschner, J. Cornil and H. J. Egelhaaf, *Adv. Mater.*, 2007, **19**, 173–191.
21 *Bruker. SADABS V2008–1*, Bruker AXS, Madison, WI, USA, 2008.
22 G. M. Sheldrick, *SHELX 97, Program for Crystal Structure Determination*, University of Göttingen, Göttingen, Germany, 1997.
23 S. Yamaguchi, R. Z. Jin, Y. Itami, T. Goto and K. Tamao, *J. Am. Chem. Soc.*, 1999, **121**, 10420–10421.
24 B. Jiang and T. D. Tilley, *J. Am. Chem. Soc.*, 1999, **121**, 9744–9745.
25 J. Roncali, F. Garnier, R. Garreau and M. Lemaire, *J. Chem. Soc., Chem. Commun.*, 1987, 1500–1502.
26 S. S. Zade and M. Bendikov, *Chem.–Eur. J.*, 2007, **13**, 3688–3700.
27 A. P. Chaloner, R. G. Sumudu and B. H. Peter, *J. Chem. Soc., Perkin Trans. 2*, 1997, 1597.
28 When the atomic positions are partially exchanged by two very different atoms in the structure, the disorder modeling becomes difficult, and more often, leads to unstable structures. Because, the higher absorption of X-rays by the heavy atom like S makes it difficult to identify the position of the lighter atom.

